electronics

Article

Digital Programmable Metasurface with Element-Independent Visible-Light Sensing

Xuqian Jiang, Fuju Ye, Hongrui Tan, Sisi Luo, Haoyang Cui and Lei Chen *

College of Electronics and Information Engineering, Shanghai University of Electric Power, No.2588 Changyang Road, Yangpu District, Shanghai 200090, China
* Correspondence: leichen_suep@163.com

Abstract: The application of jointing multiple physical field sensing with electromagnetic (EM) wave manipulation is a hot research topic recently. Refined perception and unit-level independent regulation of metasurfaces still have certain challenges. In this paper, we propose a digital programmable metasurface that can adaptively achieve various EM functions by sensing the color changes of the incident light, which enables unit-level sensing and modulation. Integrating trichromatic sensors, FPGA, and algorithm onto the metasurface has established a metasurface architecture for electromagnetic scattering field modulation from complex optics to microwave wavelengths, which enables a wide variety of light sensing for modulation. The metasurface integrated with PIN diodes and trichromatic color sensors forms a complete intelligent system of adaptive and reconfigurable coding patterns, within the pre-designed control of FPGA. We fabricated the metasurface using standard printed circuit board (PCB) technology and measured the metasurface in far-fields. The measurement results show good agreement with the simulation results, verifying our design. We envision that the proposed programmable metasurface with visible light sensing will provide a new dimension of manipulation from this perspective.

Keywords: visible-light sensing; reprogrammable; metasurface; independent regulation

Citation: Jiang, X.; Ye, F.; Tan, H.; Luo, S.; Cui, H.; Chen, L. Digital Programmable Metasurface with Element-Independent Visible-Light Sensing. *Electronics* **2023**, *12*, 241. https://doi.org/10.3390/electronics12010241

Academic Editor: Hector E. Nistazakis

Received: 22 November 2022
Revised: 26 December 2022
Accepted: 30 December 2022
Published: 3 January 2023

1. Introduction

Metamaterials [1,2] are artificial composite materials consisting of subwavelength structure that have largely improved electromagnetic (EM) [3,4] control capability. They have superior EM properties, which have led to the development of applications such as imaging [5,6], stealth [7], and negative refraction [8]. Metasurfaces [9–11], as two-dimensional versions of metamaterials, not only inherit the excellent EM properties of metamaterials, but the two-dimensional versions are easier to process and apply. As a result, metasurface research has been aroused and a wider range of EM field modulation has been realized, involving phase modulation [12–14], amplitude regulation [15–17], polarization control [18], etc.

In 2014, Prof. Cui and his team proposed digital coding programmable metamaterials/metasurfaces [19], which integrates digital information into metamaterial/metasurface design from the aspects of structure, EM parameters, and function, connecting physical worlds and digital coding worlds [20–22]. Unlike traditional metasurfaces, which perform specific functions only after the process is complete, digital coding metasurfaces allow functional reuse by reassigning the phase response of meta-atom to "0" and "1" based on numerical expressions. In addition, the digital metasurface can also introduce other regulating mechanisms according to different requests, making it more flexible and convenient. Using this approach, various digital coding metasurfaces with different functions have been proposed [23], such as amplitude coding [24,25], phase coding [26,27], polarization coding [28,29], and angular momentum coding [5,30]. More recently, intelligent metasurfaces [31–38] with adaptive reprogrammable functions without human involvement have been proposed. A typical intelligent metasurface system is a combination of sensors, control circuits, and feedback systems to form a complete, intelligent system controlled by the metasurface itself without the need for human control, such as infrared sensing [39], ultraviolet sensing [40], and thermal sensing [33]. However, previous metasurface regulation was carried out by controlling the whole metasurface or partial rows and columns of the metasurface. There are still certain challenges in the completely independent perception and regulation of metasurface units.

In this paper, we propose a digital programmable metasurface with element-independent visible-light sensing; the metasurface can be adaptively reprogrammed to achieve various EM functions by sensing the color changes of incident light. The metasurface is integrated with trichromatic color sensors (TCS3200), microcontrollers, and a preloading coding algorithm. Through the establishment of a feedback link with the programmable gate array (FPGA), the metasurface forms a complete intelligent system of adaptive and reconfigurable coding. As the proposed metasurface integrates trichromatic color sensors, it can simultaneously recognize EM waves in three frequency ranges, which is superior to the previous optical control metasurface. Notably, the system can be adaptively reprogrammed without human participation. In addition, we use light frequency to control the microwave phase. We envision that this work will further expand the degrees of freedom for metasurface sensing and manipulation, with potential applications in fields such as communications, imaging, and displays [41]. Moreover, the digital programmable metasurface also can be combined with customized control and computational programs and executive circuits to extend into the adaptive light-sensing metasurface and establish software and hardware control or intelligent meta-devices with autonomous adaptive programmable functions for the next generation of wireless systems.

2. Principle and Design

The principle of the proposed digital programmable metasurface is shown in Figure 1a. The metasurface consists of 16×16 meta-cells, with four meta-atoms in a group, each group integrating a trichromatic sensor and microcircuit. Note that the algorithm links the process of light-sensing metasurfaces from detection to sensory data, data comparison, and finally the formation of different voltage distribution patterns on the metasurface. Specifically, when the frequency information of the light is sensed by the trichromatic sensors and output to the high-speed ADC, the ADC determines whether the threshold is exceeded, and then the FPGA makes the threshold judgment and controls the PIN diode on the metasurface to perform the coding patterns of the color corresponding to the current threshold value. For instance, when the FPGA determines that the incident light is red, the metasurface performs the coding pattern of dual-beam; when the incident light is green, the metasurface performs the coding pattern of four-beam; and when the incident light is red, the metasurface performs the coding pattern of RCS. In addition, in order to show more clearly how our proposed metasurface works, we provide a schematic illustration, as shown in Figure 1b.

To verify our idea, we designed four metasurfaces; Figure 2 shows a three-dimensional graph of a trichromatic-color-sensing meta-cell. The metamaterial unit has three layers. The first layer is a metal patch, the middle layer is an FR-4 layer with a dielectric constant of 4.3 and a dielectric loss angle of 0.025, and the bottom layer is a metal ground. To achieve dynamic unit tunability, we embedded a PIN diode (Skyworks SMP1320) between two symmetrical metal patches in the first layer. In addition, to connect the control circuit, we set two through-holes with a diameter of 0.15 mm on the unit. In the process of simulation verification using CST Microwave Studio, the EM metamaterial unit model (shown in Figure 2a) was established with a period p of 14 mm, a thickness of medium h of 3.5 mm, and a thickness of metal patch of 0.1 mm. Other parameters are shown as follows: a = 12 mm, w = 3 mm, w1 = 4.5 mm, l = 1.7 mm, and l1 = 4.5 mm. PIN diodes are equivalent, using a resist-inductor-capacitor (RLC) model, and the diode equivalent diagram is shown in Figure 2b. The code “0” indicates that the PIN diode is in the OFF state, with R1 = 0, L1 = 0.4 nH, and C1 = 0.4 pF. The code "1" indicates that the PIN diode is in the ON state, with R2 = 2.2, L2 = 0.4 nH, and C2 = 0 pF. The amplitude and phase curves of the metamaterial element under y-polarization are shown in Figure 2c,d. At the frequency point of 4.1 GHz, the phase difference between the two states of the element is π, and the amplitudes of the two states are -0.27 dB and -0.99 dB, respectively, showing that the metasurface wavefront is well manipulated [19].

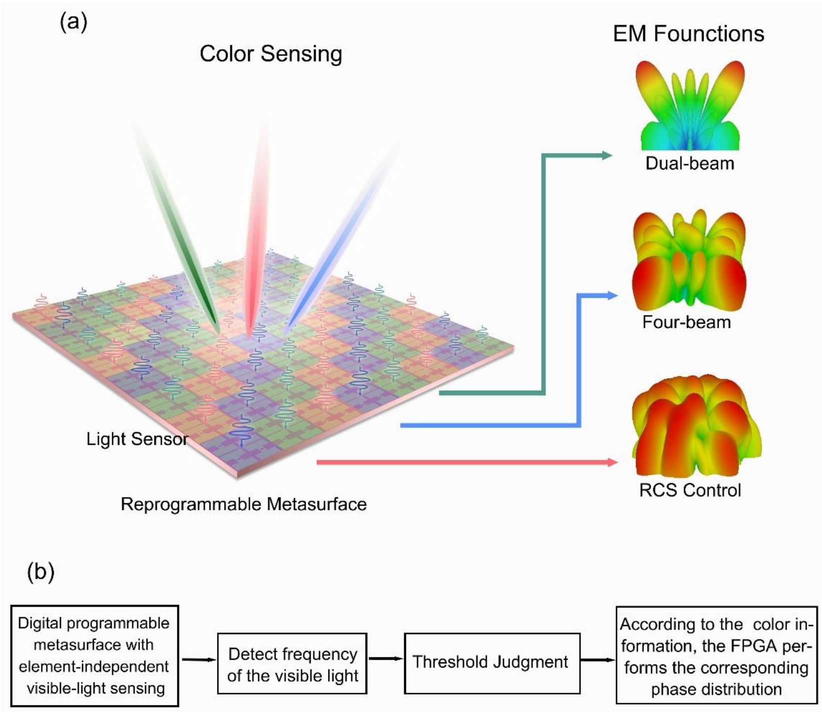

Figure 1. (**a**) Schematic illustration of the digital programmable metasurface. When the digital programmable metasurface detects different color information, its reflection phase patterns will be reprogrammed. (**b**) Illustration of the working principle.

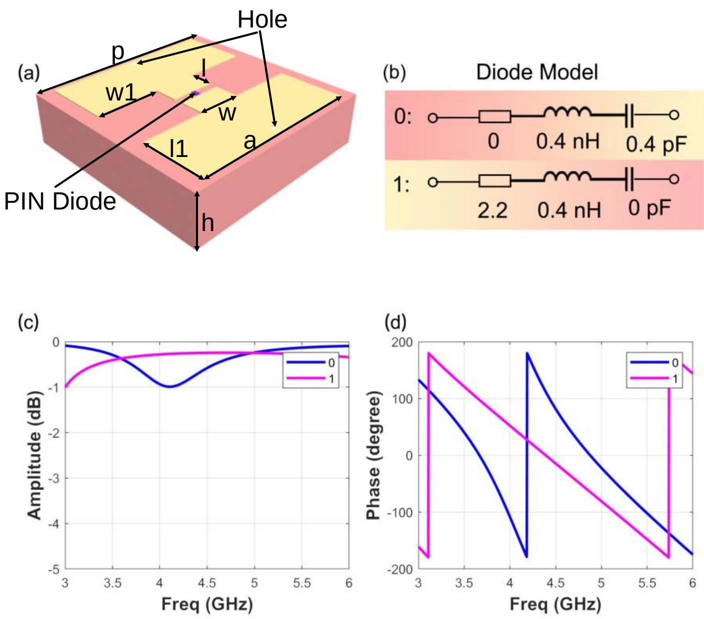

Figure 2. Description of the structure and EM response of meta-atom. (**a**) Three-dimensional perspective view of the supercell. (**b**) Equivalent circuit of PIN diode in OFF/ON state. (**c**) Magnitude-response of the element. (**d**) Phase-response of the element.

To achieve independent control of small areas of the metamaterial, and to obtain EM control that is more accurate, we used PCB technology to add an isolation layer and a control circuit layer based on the original metasurface. The resulting complete structure consisted of five layers, as Figure 2b shows. The dielectric layer was designed to isolate, and the circuit layer was designed to control the small area of the metasurface independently. In Figure 3, we show the stereoscopic graph of the meta-atom group structure. The circuit layer is covered with 2 × 2 metamaterial cells in order from left to right. In addition, the microcircuit and the metasurface are connected through the vias to realize the metasurface control mode that is controlled by "point". Figure 3c shows the circuit structure of the sensing module. In the trichromatic sensor, the light-to-frequency converter reads an 8 × 8 array of photodiodes; 16 photodiodes have blue filters, 16 photodiodes have green filters, 16 photodiodes have red filters, and 16 photodiodes are clear with no filters. Four colors of photodiodes are connected to reduce the effect of uneven incident irradiance. Through control of the digital state of the enabling ports SH2 and SH3, the sensing target is converted to one of the colors of the enabling port, and the result is output at a certain frequency. A trichromatic sensor sample is shown in Figure 3d, and Figure 3c shows the 8 × 8 photodiodes array. In this work, the sensing modules are integrated into the fifth layer using PCB technology, and the modules are connected to PIN on the metasurface through the vias. The integration of trichromatic sensors on the metasurface allows the color information in incident light to be detected; this can also be regarded as a light-coding input to guide the metasurface to perform corresponding functions. For example, we marked the implementation of electromagnetic functions, such as dual-beam, four-beam, and RCS, as detecting blue, green, and red, respectively. As prototype proof, according to the theoretical knowledge of coding metasurface [19], four typical coding patterns were selected for simulation and measurement verification to prove the above ideas.

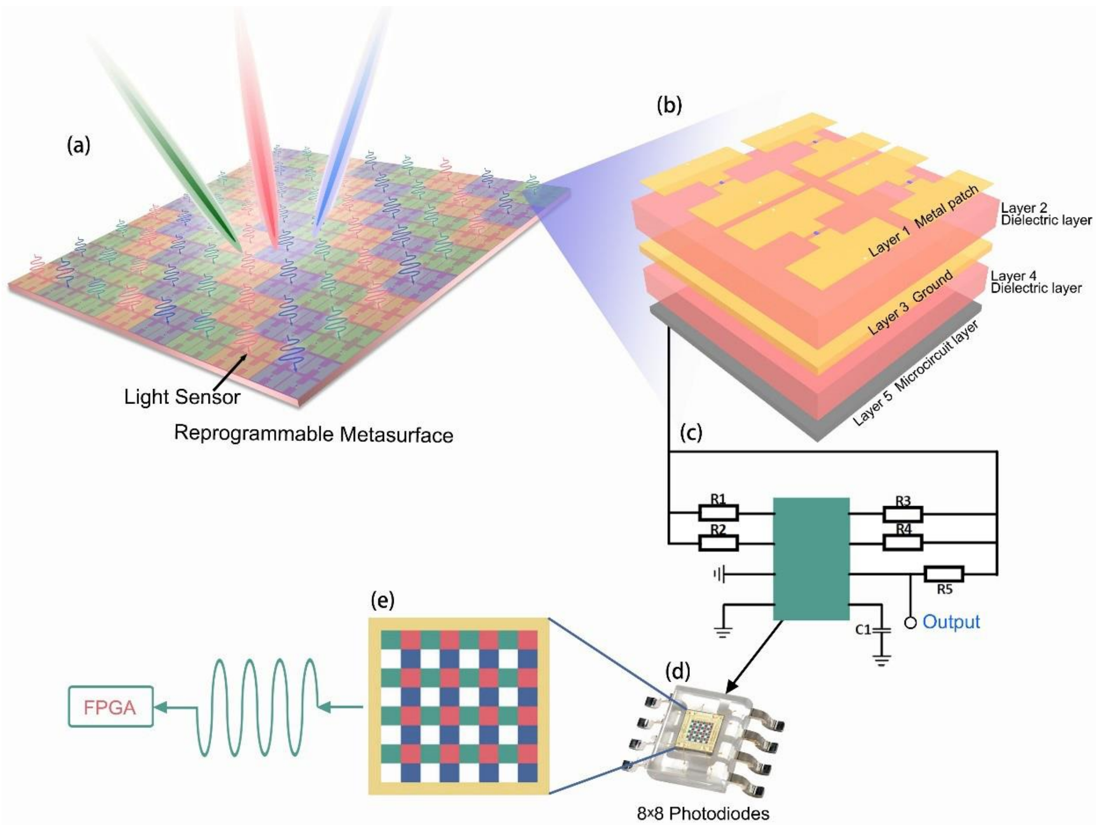

Figure 3. The stereoscopic graph of the meta-atom group structure. (**a**) The digital programmable metasurface. (**b**) The stereoscopic graph structure consists of four meta-atoms. (**c**) Microcontroller module. (**d**) A sample of the color sensor. (**e**) Light-to-frequency converter. The light-to-frequency converter reads an 8 × 8 array of photodiodes.

3. Results

To verify the above ideas, we designed metasurface arrays with the coding "0000111100001111", "0001111100000111", a chessboard metasurface with the code "0001111100000111", and a randomly coding RCS reduction metasurface. Figure 4 shows the far-field simulation results of the above four metasurfaces. We marked the metasurface array with the codes "0000111100001111" as pattern A, the metasurface array with the codes "0001111100000111" as pattern B, the chessboard metasurface as pattern C, and the RCS metasurface as pattern D. Figure 4e–h show the far-field simulation results of patterns A–D at 4.1 GHz, and Figure 4i–l show the two-dimensional display of far-field results of patterns A–D at 4.1 GHz. The above results show that patterns A and B realized dual-beam scattering with different pointing angles under normal electromagnetic irradiation. The scattering angle of pattern A was approximately 39° and its beam energy was approximately 3.2 dB; the scattering angle of pattern B was approximately 34° and its beam energy was approximately 3.7 dB. Pattern C achieved four-beam scattering with good symmetry. Pattern D implemented RCS reduction.

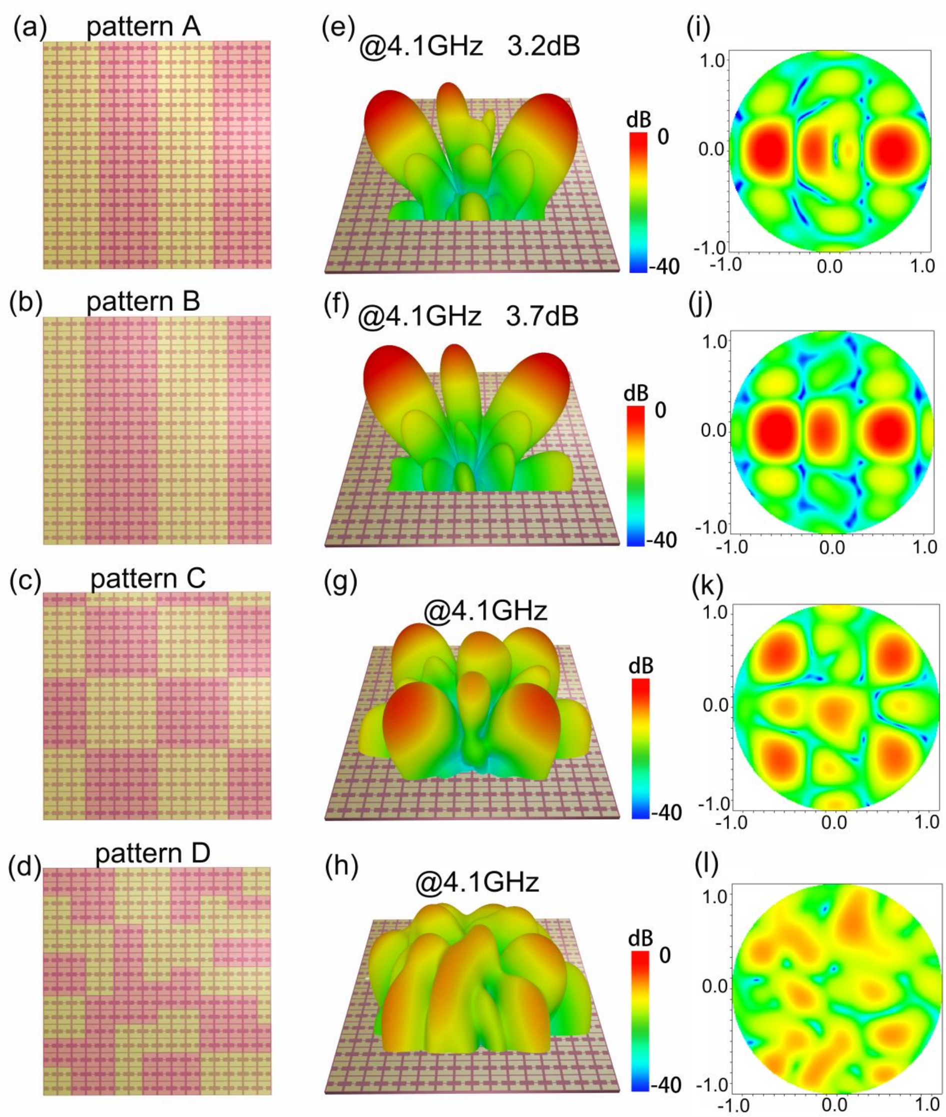

Figure 4. Four coding patterns of the metasurface and their corresponding far-field results. (**a**) Pattern A coding as "0000111100001111". (**b**) Pattern B coding as "0000111100001111". (**c**) Pattern C horizontal coding as "00011110000111". (**d**) Pattern D is randomly coding. (**e**–**h**) Far-field simulation results of patterns A–D at 4.1 GHz. (**i**–**l**) Two-dimensional displays of far-field results of patterns A–D at 4.1 GHz.

The generalized Snell's law [19,42,43] is to arrange the units with different abrupt phases in a gradient or a specific phase distribution on a plane, which can realize the functions of anomalous deflection (negative reflection) [44], anomalous reflection [45], and focusing the incident electromagnetic waves [46,47]. When this design idea is applied to a 1-bit coding metasurface [48], two units with 180° phase difference are encoded as "0" and "1", and these two units are arranged on a two-dimensional plane in a predetermined sequence, forming a metasurface with a regulatory function for electromagnetic waves. For example, when the coding sequence is "0101 . . . ", the vertically incident electromagnetic waves will be divided into dual-beam, and when the coding becomes a checkerboard distribution, the radiation direction will form as four beams. Our proposed pattern A, with the code "11100001111000", and pattern B, with the code "11000001111100", were both dual-beam. The simulation results of pattern C, with "11100001111000" chessboard coding, were indeed four beams; that is, our results were consistent with the theory, which proves the feasibility of our proposed light-sensing coding metasurface.

Figure 5 shows the sample of the metasurface and the far-field experimental results. Figure 5a shows the fabricated metasurface sample, with a metasurface composed of 16 × 16 cells. There were four meta-atoms in a group, and each group integrated a trichromatic sensor and microcontroller. The trichromatic sensor and micro control module were connected to a 1-bit coding metasurface. As illustrated in Figure 5a, to realize the flexible and independent regulation of each meta-atom group, a light-tight plastic sheet was inserted between the groups to prevent interference from light information.

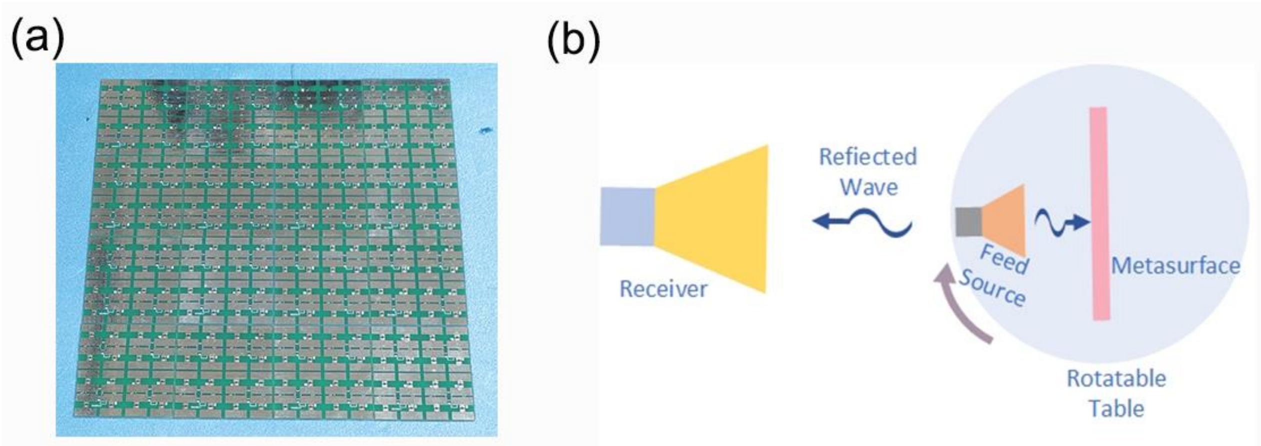

Figure 5. The sample of the metasurface and the measurement configuration for the far-field test. (**a**) The metasurface is composed of 16 × 16 units. (**b**) The measurement configuration for the far-field test.

In the experimental demonstration, we fabricated the metasurface and verified the far-field results in a standard microwave chamber. The measuring device is shown in Figure 5b. The fabricated metasurface sample and feed source were fixed on a rotatable table. Two rectangular horn antennas were used as the feed and receiver, respectively. When the rotatable table rotated, the far-field data on the two-dimensional plane could be measured. To obtain quasi-plane waves, the source antenna was placed 1 m away from the metasurface sample, while the receiver was placed 10 m away from the turntable.

To compare the measured and simulated results more intuitively, the results of both were recorded as shown in Figure 6a–c. The simulated and measured data were identified using blue and red colors, respectively. The dual-beam feature or the four-beam feature can clearly be seen in the figures, and the simulation and the measured beam features were in good agreement. Furthermore, the simulated and measured blue and red lines had approximately the same trends, demonstrating a high degree of consistency between the measured and simulated results. The minor measurement deviation between the simulated and measured results was primarily owing to the manual operation of the experiments and manufacturing errors. There are other reasons for the extra reflection of the light control module and the non-ideal excitation of the horn antenna.

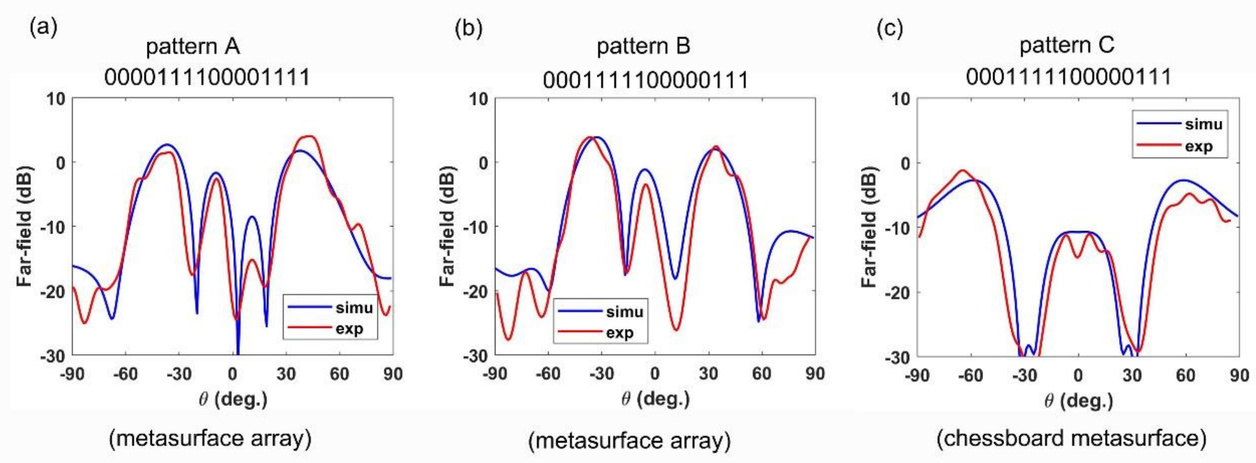

Figure 6. The far-field experimental results of three patterns. (**a**–**c**) present a comparison of far-field simulation and the experimental results of patterns A, B, and C, respectively.

4. Conclusions

This paper presents a digital programmable metasurface with element-independent visible-light sensing. The metasurface consists of 16 × 16 units, with four meta-units in a group, each group integrating a trichromatic sensor and microcontroller. The trichromatic sensor and micro control module are connected to a 1-bit coding metasurface. The light field distribution can be regulated by controlling these meta-atom groups independently. The metasurface obtains different coding sequences according to changes in optical frequency, and dynamically modulates the reflected phase to produce different beam deflections. Three patterns were designed to verify the performance of the metasurface. The results show that analog and measurement results have good consistency. In this work, we have achieved a wide range of electromagnetic modulations, such as dual-beam, four-beam, and RCS, as well as color detection of incident light, by integrating trichromatic color sensors, high-speed ADC, FPGA, and algorithms onto a metasurface. Moreover, we have established a metasurface architecture for electromagnetic scattering field modulation from complex optics to microwave wavelengths, which enables a wide variety of light sensing for modulation. This is valuable for developing hybrid electronic-photonic devices for more advanced electronic and communication systems. We believe that our study will broaden the degrees of freedom for metasurface sensing and manipulation, with possible applications in communications, imaging, and displays.

Author Contributions: Conceptualization, X.J. and H.T.; methodology, X.J.; software, F.Y.; validation, S.L., F.Y. and H.T.; formal analysis, X.J.; investigation, H.C.; writing—original draft preparation, H.T.; writing—review and editing, H.C.; visualization, S.L.; project administration, X.J.; funding acquisition, L.C. All authors have read and agreed to the published version of the manuscript.

Funding: This work was funded by the National Key Research and Development Program of the National Natural Science Foundation of China (grant numbers 11404207 and 52177185), the SHIEP Foundation (grant numbers K2014-054 and Z2015-086), and the Local Colleges and Universities Capacity Building Program of the Shanghai Science and Technology Committee, China (grant number 15110500900).

Data Availability Statement: The data that support the findings of this study are available on request form the corresponding author.

Conflicts of Interest: The authors declare no conflict of interest.

References

1. El Dhaba, A.R. Reduced micromorphic model in orthogonal curvilinear coordinates and its application to a metamaterial hemisphere. *Sci. Rep.* **2020**, *10*, 2846. [CrossRef] [PubMed]
2. Grbic, A.; Eleftheriades, G.V. Experimental verification of backward-wave radiation from a negative refractive index metamaterial. *J. Appl. Phys.* **2002**, *92*, 5930–5935. [CrossRef]
3. Pendry, J.B.; Schurig, D.; Smith, D.R. Controlling electromagnetic fields. *Science* **2006**, *312*, 1780–1782. [CrossRef]
4. Hao, J.; Yuan, Y.; Ran, L.; Jiang, T.; Kong, J.A.; Chan, C.T.; Zhou, L. Manipulating electromagnetic wave polarizations by anisotropic metamaterials. *Phys. Rev. Lett.* **2007**, *99*, 063908. [CrossRef] [PubMed]
5. Xiao, Q.; Ma, Q.; Yan, T.; Wu, L.W.; Liu, C.; Wang, Z.X.; Wan, X.; Cheng, Q.; Cui, T.J. Orbital-Angular-Momentum-Encrypted Holography Based on Coding Information Metasurface. *Adv. Opt. Mater.* **2021**, *9*, 2002155. [CrossRef]
6. Fang, N.; Lee, H.; Sun, C.; Zhang, X. Sub-diffraction-limited optical imaging with a silver superlens. *Science* **2005**, *308*, 534–537. [CrossRef]
7. Ma, Q.; Mei, Z.L.; Zhu, S.K.; Jin, T.Y.; Cui, T.J. Experiments on Active Cloaking and Illusion for Laplace Equation. *Phys. Rev. Lett.* **2013**, *111*, 173901. [CrossRef] [PubMed]
8. Shelby, R.A.; Smith, D.R.; Schultz, S. Experimental verification of a negative index of refraction. *Science* **2001**, *292*, 77–79. [CrossRef]
9. Falcone, F.; Lopetegi, T.; Laso, M.A.G.; Baena, J.D.; Bonache, J.; Beruete, M.; Marques, R.; Martin, F.; Sorolla, M. Babinet principle applied to the design of metasurfaces and metamaterials. *Phys. Rev. Lett.* **2004**, *93*, 197401. [CrossRef]
10. Alu, A. Mantle cloak: Invisibility induced by a surface. *Phys. Rev. B* **2009**, *80*, 245115. [CrossRef]
11. Wu, H.; Bai, G.D.; Liu, S.; Li, L.; Wan, X.; Cheng, Q.; Cui, T.J. Information theory of metasurfaces. *Natl. Sci. Rev.* **2020**, *7*, 561–571. [CrossRef] [PubMed]
12. Liu, S.; Cui, T.J.; Xu, Q.; Bao, D.; Du, L.; Wan, X.; Tang, W.X.; Ouyang, C.; Zhou, X.Y.; Yuan, H.; et al. Anisotropic coding metamaterials and their powerful manipulation of differently polarized terahertz waves. *Light Sci. Appl.* **2016**, *5*, e16076. [CrossRef] [PubMed]
13. Chen, L.; Ma, Q.; Luo, S.S.; Ye, F.J.; Cui, H.Y.; Cui, T.J. Touch-Programmable Metasurface for Various Electromagnetic Manipulations and Encryptions. *Small* **2022**, *18*, 2203871. [CrossRef] [PubMed]
14. Ma, Q.; Hong, Q.R.; Gao, X.; Xiao, Q.; Chen, L.; Cui, T.J. Highly integrated programmable metasurface for multifunctions in reflections and transmissions. *APL Mater.* **2022**, *10*, 061113. [CrossRef]
15. Bao, L.; Ma, Q.; Bai, G.D.; Jing, H.B.; Wu, R.Y.; Fu, X.J.; Yang, C.; Wu, J.W.; Cui, T.J. Design of digital coding metasurfaces with independent controls of phase and amplitude responses. *Appl. Phys. Lett.* **2018**, *113*, 063502. [CrossRef]
16. Yang, Y.; Jing, L.; Zheng, B.; Hao, R.; Yin, W.; Li, E.; Soukoulis, C.M.; Chen, H. Full-Polarization 3D Metasurface Cloak with Preserved Amplitude and Phase. *Adv. Mater.* **2016**, *28*, 6866–6871. [CrossRef] [PubMed]
17. Ma, Q.; Chen, L.; Jing, H.B.; Hong, Q.R.; Cui, H.Y.; Liu, Y.; Li, L.L.; Cui, T.J. Controllable and Programmable Nonreciprocity Based on Detachable Digital Coding Metasurface. *Adv. Opt. Mater.* **2019**, *7*, 1901285. [CrossRef]
18. Ma, Q.; Shi, C.B.; Bai, G.D.; Chen, T.Y.; Noor, A.; Cui, T.J. Beam-Editing Coding Metasurfaces Based on Polarization Bit and Orbital-Angular-Momentum-Mode Bit. *Adv. Opt. Mater.* **2017**, *5*, 1700548. [CrossRef]
19. Cui, T.J.; Qi, M.Q.; Wan, X.; Zhao, J.; Cheng, Q. Coding metamaterials, digital metamaterials and programmable metamaterials. *Light Sci. Appl.* **2014**, *3*, e218. [CrossRef]
20. Ma, Q.; Xiao, Q.; Hong, Q.R.; Gao, X.; Galdi, V.; Cui, T.J. Digital Coding Metasurfaces: From Theory to Applications. *IEEE Antennas Propag. Mag.* **2022**, *64*, 96–109. [CrossRef]
21. Ma, Q.; Liu, C.; Xiao, Q.; Gu, Z.; Gao, X.X.; Li, L.; Cui, T.J. Information metasurfaces and intelligent metasurfaces. *Photonics Insights* **2022**, *1*, R01. [CrossRef]
22. Ma, Q.; Cui, T.J. Information Metamaterials: Bridging the physical world and digital world. *PhotoniX* **2020**, *1*, 1. [CrossRef]
23. You, J.W.; Ma, Q.; Lan, Z.; Xiao, Q.; Panoiu, N.C.; Cui, T.J. Reprogrammable plasmonic topological insulators with ultrafast control. *Nat. Commun.* **2021**, *12*, 5468. [CrossRef] [PubMed]
24. Hong, Q.R.; Ma, Q.; Gao, X.X.; Liu, C.; Xiao, Q.; Iqbal, S.; Cui, T.J. Programmable Amplitude-Coding Metasurface with Multifrequency Modulations. *Adv. Intell. Syst.* **2021**, *3*, 2000260. [CrossRef]
25. Luo, J.; Ma, Q.; Jing, H.; Bai, G.; Wu, R.; Bao, L.; Cui, T. 2-bit amplitude-modulated coding metasurfaces based on indium tin oxide films. *J. Appl. Phys.* **2019**, *126*, 113102. [CrossRef]
26. Chen, K.; Feng, Y.; Yang, Z.; Cui, L.; Zhao, J.; Zhu, B.; Jiang, T. Geometric phase coded metasurface: From polarization dependent directive electromagnetic wave scattering to diffusion-like scattering. *Sci. Rep.* **2016**, *6*, 35968. [CrossRef]
27. Wu, R.Y.; Zhang, L.; Bao, L.; Wu, L.W.; Ma, Q.; Bai, G.D.; Wu, H.T.; Cui, T.J. Digital Metasurface with Phase Code and Reflection-Transmission Amplitude Code for Flexible Full-Space Electromagnetic Manipulations. *Adv. Opt. Mater.* **2019**, *7*, 1801429. [CrossRef]
28. Chen, L.; Ma, Q.; Nie, Q.F.; Hong, Q.R.; Cui, H.Y.; Ruan, Y.; Cui, T.J. Dual-polarization programmable metasurface modulator for near-field information encoding and transmission. *Photonics Res.* **2021**, *9*, 116. [CrossRef]
29. Ma, Q.; Hong, Q.R.; Bai, G.D.; Jing, H.B.; Wu, R.Y.; Bao, L.; Cheng, Q.; Cui, T.J. Editing Arbitrarily Linear Polarizations Using Programmable Metasurface. *Phys. Rev. Appl.* **2020**, *13*, 021003. [CrossRef]
30. Ding, G.; Chen, K.; Luo, X.; Zhao, J.; Jiang, T.; Feng, Y. Dual-Helicity Decoupled Coding Metasurface for Independent Spin-to-Orbital Angular Momentum Conversion. *Phys. Rev. Appl.* **2019**, *11*, 044043. [CrossRef]

31. Ma, Q.; Hong, Q.R.; Gao, X.X.; Jing, H.B.; Liu, C.; Bai, G.D.; Cheng, Q.; Cui, T.J. Smart sensing metasurface with self-defined functions in dual polarizations. *Nanophotonics* **2020**, *9*, 3271–3278. [CrossRef]
32. Chen, L.; Nie, Q.F.; Ruan, Y.; Luo, S.S.; Ye, F.J.; Cui, H.Y. Light-controllable metasurface for microwave wavefront manipulation. *Opt Express* **2020**, *28*, 18742–18749. [CrossRef] [PubMed]
33. Chen, L.; Nie, Q.F.; Ruan, Y.; Cui, H.Y. Thermal sensing metasurface with programmable wave-front manipulation. *J. Appl. Phys.* **2020**, *128*, 075105. [CrossRef]
34. Ma, Q.; Gao, W.; Xiao, Q.; Ding, L.; Gao, T.; Zhou, Y.; Gao, X.; Yan, T.; Liu, C.; Gu, Z.; et al. Directly wireless communication of human minds via non-invasive brain-computer-metasurface platform. *eLight* **2022**, *2*, 11. [CrossRef]
35. Liu, C.; Ma, Q.; Luo, Z.J.; Hong, Q.R.; Xiao, Q.; Zhang, H.C.; Miao, L.; Yu, W.M.; Cheng, Q.; Li, L.; et al. A programmable diffractive deep neural network based on a digital-coding metasurface array. *Nat. Electron.* **2022**, *5*, 113–122. [CrossRef]
36. Gu, Z.; Ma, Q.; Liu, C.; Xiao, Q.; Gao, X.; Yan, T.; Miao, L.; Li, L.; Cui, T.J. High-Resolution Programmable Metasurface Imager Based on Multilayer Perceptron Network. *Adv. Opt. Mater.* **2022**, *10*, 2200619. [CrossRef]
37. Ma, Q.; Bai, G.D.; Jing, H.B.; Yang, C.; Li, L.; Cui, T.J. Smart metasurface with self-adaptively reprogrammable functions. *Light Sci. Appl.* **2019**, *8*, 98. [CrossRef]
38. Goi, E.; Zhang, Q.; Chen, X.; Luan, H.; Gu, M. Perspective on photonic memristive neuromorphic computing. *PhotoniX* **2020**, *1*, 3. [CrossRef]
39. Nguyen Thanh, T.; Tanaka, T. Characterizations of an infrared polarization-insensitive metamaterial perfect absorber and its potential in sensing applications. *Photonics Nanostruct. Fundam. Appl.* **2018**, *28*, 100–105. [CrossRef]
40. Chen, L.; Ye, F.J.; Cuo, M.; Luo, S.S.; Hao, J.J.; Ruan, Y.; Cui, H.Y. Ultraviolet-sensing metasurface for programmable electromagnetic scattering field manipulation by combining light control with a microwave field. *Opt Express* **2022**, *30*, 19221. [CrossRef]
41. Zhan, T.; Xiong, J.; Zou, J.; Wu, S.-T. Multifocal displays: Review and prospect. *PhotoniX* **2020**, *1*, 10. [CrossRef]
42. Leonhardt, U. Optical conformal mapping. *Science* **2006**, *312*, 1777–1780. [CrossRef] [PubMed]
43. Yu, N.F.; Genevet, P.; Kats, M.A.; Aieta, F.; Tetienne, J.P.; Capasso, F.; Gaburro, Z. Light Propagation with Phase Discontinuities: Generalized Laws of Reflection and Refraction. *Science* **2011**, *334*, 333–337. [CrossRef] [PubMed]
44. Della Giovampaola, C.; Engheta, N. Digital metamaterials. *Nat. Mater.* **2014**, *13*, 1115. [CrossRef] [PubMed]
45. Liu, S.; Noor, A.; Du, L.L.; Zhang, L.; Xu, Q.; Luan, K.; Wang, T.Q.; Tian, Z.; Tang, W.X.; Han, J.G.; et al. Anomalous Refraction and Nondiffractive Bessel-Beam Generation of Terahertz Waves through Transmission-Type Coding Metasurfaces. *Acs Photonics* **2016**, *3*, 1968–1977. [CrossRef]
46. Li, L.; Cui, T.J.; Ji, W.; Liu, S.; Ding, J.; Wan, X.; Li, Y.B.; Jiang, M.; Qiu, C.-W.; Zhang, S. Electromagnetic reprogrammable coding-metasurface holograms. *Nat. Commun.* **2017**, *8*, 197. [CrossRef]
47. Yang, H.; Cao, X.; Yang, F.; Gao, J.; Xu, S.; Li, M.; Chen, X.; Zhao, Y.; Zheng, Y.; Li, S. A programmable metasurface with dynamic polarization, scattering and focusing control. *Sci. Rep.* **2016**, *6*, 35692. [CrossRef]
48. Liu, S.; Cui, T.J.; Zhang, L.; Xu, Q.; Wang, Q.; Wan, X.; Gu, J.Q.; Tang, W.X.; Qi, M.Q.; Han, J.G.; et al. Convolution Operations on Coding Metasurface to Reach Flexible and Continuous Controls of Terahertz. *Adv. Sci.* **2016**, *3*, 1600156. [CrossRef]